

Cu₂O Microcrystals Grown on Silicon as Platform for Quantum-Degenerate Excitons and Rydberg States

Stephan Steinhauer^{1,*}, Marijn A. M. Versteegh¹, André Mysyrowicz², Birgit Kunert³, and Val Zwiller¹

¹Department of Applied Physics, KTH Royal Institute of Technology, SE-100 44 Stockholm, Sweden

²Laboratoire d'Optique Appliquée, ENSTA ParisTech, CNRS, Ecole Polytechnique, F-91762 Palaiseau, France

³Institute of Solid State Physics, Graz University of Technology, A-8010 Graz, Austria

*e-mail: ssteinh@kth.se

ABSTRACT

Cuprous oxide (Cu₂O) is a semiconductor with large exciton binding energy and significant technological importance in applications such as photovoltaics and solar water splitting. It is also a superior material system for quantum optics that enabled the observation of two intriguing phenomena, i.e. Rydberg excitons as solid-state analogue to highly-excited atomic states and dense exciton gases showing quantum degeneracy when approaching the phase transition to Bose-Einstein condensation. Previous experiments focused on natural bulk crystals due to major difficulties in growing high-quality synthetic samples. Here, we present Cu₂O microcrystals with excellent optical material quality capable of hosting both quantum-degenerate excitons and excited Rydberg states. Growth of Cu₂O with exceedingly low point defect levels was achieved on silicon by a scalable thermal oxidation process compatible with lithographic patterning. Using the latter, we demonstrate Rydberg excitons in site-controlled Cu₂O microstructures, paving the way for a plethora of applications in integrated quantum photonics.

Light-matter interactions in the direct-band-gap semiconductor cuprous oxide (Cu₂O) are widely governed by excitons, quasi-particles arising from electron-hole Coulomb interactions, which can be observed up to room temperature due to their large binding energy. As a result of the unique excitonic properties, intriguing condensed-matter quantum phenomena have been demonstrated, e.g. quantum-degenerate exciton gases^{1,2} and giant Rydberg excitons³ exhibiting signatures of quantum coherences⁴ and quantum chaotic behavior⁵. As the exciton ground state - the so-called paraexciton - is decoupled from the radiation field in unstrained Cu₂O, paraexcitons can reach lifetimes up to microseconds rendering them a prime candidate for excitonic Bose-Einstein condensation⁶. Apart from quantum optics, recent reports have reinforced the significant potential of Cu₂O as a low-cost, non-toxic material in areas such as photocatalysis⁷, solar water splitting⁸ and photovoltaic devices⁹. Various methods have been reported for the growth of Cu₂O thin films and single crystals¹⁰, in particular molecular beam epitaxy^{11,12}, vapor phase transport¹³, magnetron sputtering¹⁴ in combination with thermal annealing¹⁵, thermal oxidation¹⁶ and the floating zone method¹⁷. However, state-of-the-art quantum optics experiments still focus on natural bulk crystals originating from mines, clearly underlining that significant progress in Cu₂O growth is required to surpass inherent limitations of natural samples. Recent literature emphasized that for the observation of Rydberg states with principal quantum numbers higher than the current record value of $n=25$ samples with lower impurity concentrations are required¹⁸. In addition, scalable fabrication techniques suitable for obtaining micro- / nanostructures and compatible with standard silicon processing are needed to deploy the full potential of this material in advanced device technologies, for instance integrated quantum photonic circuits.

In this work, we present Cu₂O growth on silicon by a scalable thermal oxidation process, which resulted in high-quality microcrystal structures with exceedingly low point defect and impurity levels. We achieve a dense exciton gas in single Cu₂O microcrystals at milli-Kelvin temperatures under continuous-wave excitation, showing quantum degeneracy close to the phase boundary to Bose-Einstein condensation. Furthermore, we demonstrate luminescence from excited np Rydberg states in lithographically site-controlled structures, exhibiting excellent agreement with a hydrogen-like quantum number dependence. Due to the exceptional optical material quality and the unique excitonic properties, our Cu₂O microcrystals are highly promising for enabling new photonic device architectures relevant for quantum information processing and quantum sensing.

Growth and structural/photoluminescence properties

The growth of Cu₂O microcrystals relied on a scalable single-step thermal oxidation process schematically depicted in Fig. 1a. Copper films (thickness ~ 700 nm) were deposited by electron beam evaporation on silicon substrates covered with a thermal SiO₂ layer. Thermal oxidation in a tube furnace resulted in Cu₂O films with microcrystalline morphology, which can be seen in

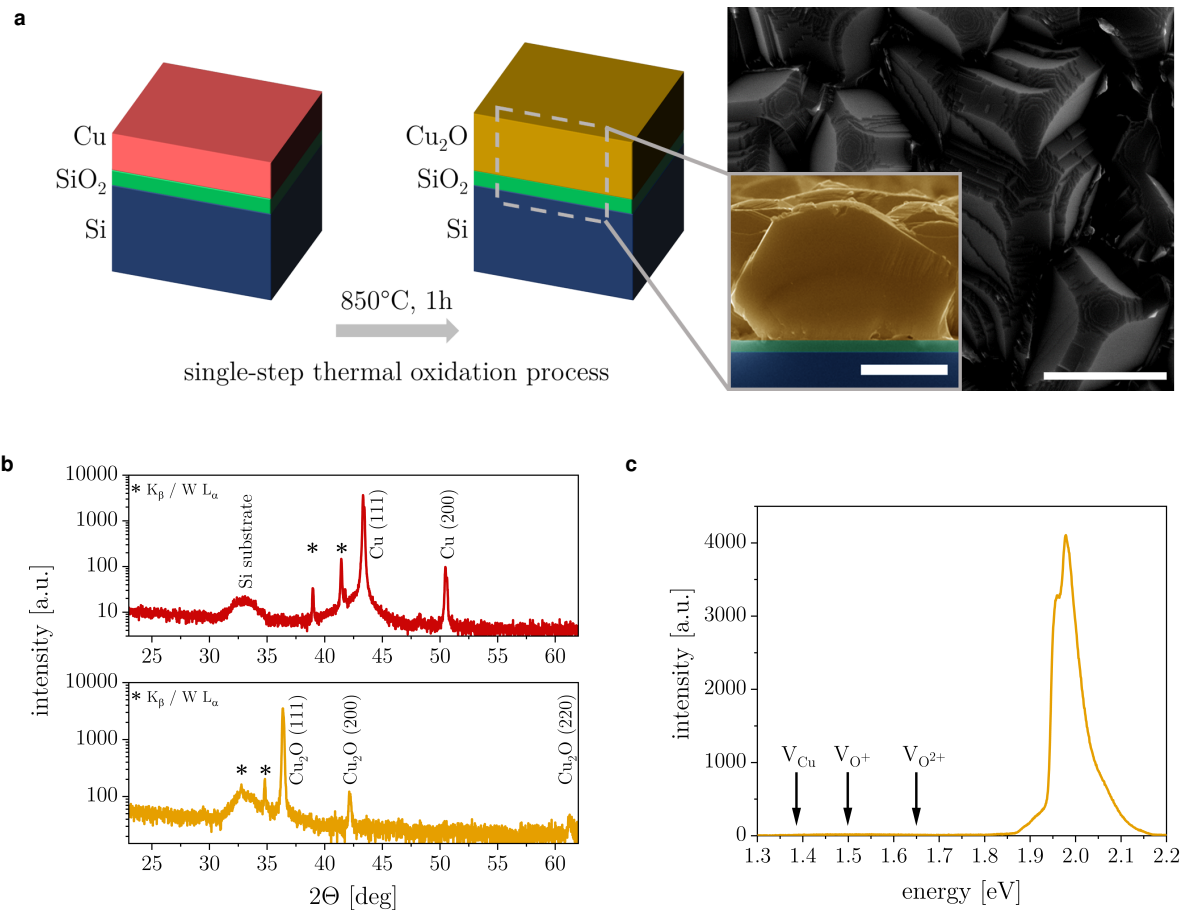


Fig.1 | Growth and characterization of Cu_2O microcrystals. a, Schematics of sample layer structure before and after the thermal oxidation process (left). Top-view scanning electron micrograph of Cu_2O microcrystals after thermal oxidation at 850°C for 1 h at pressures of 1 mbar synthetic air (right); the bottom inset shows a corresponding cross-sectional image (scale bars $1\ \mu\text{m}$). **b**, X-ray diffraction of as-deposited copper film (top) and Cu_2O film after thermal oxidation (bottom). **c**, Room-temperature photoluminescence spectroscopy of Cu_2O microcrystal under continuous-wave laser excitation (532 nm). The emission around 2 eV is due to the recombination of free excitons.

the top-view and cross-sectional scanning electron microscopy images. The Cu_2O microcrystals showed terrace-like structures on the surface (Supplementary Fig.S1) and faceted grains with sizes in the μm range. As-deposited copper and samples after thermal oxidation to Cu_2O were characterized by X-ray diffraction (XRD) measurements (Fig.1b) to determine their phase composition. For as-deposited copper, the expected face-centered cubic structure and texturing along the [111] direction was found. The presented single-step thermal oxidation method resulted in phase-pure Cu_2O with cubic cuprite structure. For samples fabricated with different growth conditions comparable microcrystal morphology as well as similar XRD results were obtained (Supplementary Fig.S2). Thermal oxidation of copper can lead to different oxide phases¹⁰; Cu_2O growth was reported to proceed via the random nucleation of islands, which exhibit a cube-on-cube epitaxial relationship at the metal-oxide interface (low oxygen partial pressures)¹⁹ or non-epitaxial orientations (above critical oxygen partial pressures depending on the copper surface)²⁰. For the range of experimental parameters corresponding to the growth conditions used in this study ($800\text{-}850^\circ\text{C}$, $p\sim 1$ mbar of synthetic air) the initial stages of copper oxidation include epitaxial oxide formation accompanied by rapid two-dimensional growth²¹. The XRD results before and after thermal oxidation (Fig.1b) show pronounced texturing in {111} direction in both cases, indicating that the oxidation proceeds via an epitaxial relationship of Cu_2O {111} \parallel Cu {111}. This relationship is in accordance with literature reports on the thermal oxidation of copper thin films¹⁹ and nanoparticles with sizes down to few nanometers²². Similar to a previous report on epitaxial Cu_2O growth on MgO ¹⁴, the observed terrace-like structures on the Cu_2O surfaces are suggesting a two-dimensional growth mode for individual microcrystals.

The optical material quality of the Cu_2O microcrystals was initially assessed by means of room-temperature photoluminescence spectroscopy. Distinct free exciton emission was observed (Fig.1c), exhibiting a characteristic lineshape resulting from multiple phonon-assisted recombination processes with spectral overlap¹¹. At photon energies attributed to copper vacancies or single/double-charged oxygen vacancies¹⁰ no marked luminescence was observed. Additional data for microcrystalline

Cu₂O films from different batches and grown under different conditions can be found in Supplementary Fig.S3, which shows spectra with very similar characteristics. Hence, the presented single-step thermal oxidation process is a robust method for the realization of microcrystalline Cu₂O films with excellent optical material quality.

Point defects, bound excitons and yellow 1s excitons

Local deviations from the ideal cuprite crystalline structure, e.g. vacancy point defects, extrinsic impurities or microscopic strain, have a significant impact on the relaxation of excitons in Cu₂O and the related photon emission. Photoluminescence spectroscopy experiments were conducted in a dilution refrigerator (sample stage base temperature around 40 mK) to assess the optical material quality of Cu₂O microcrystals at milli-Kelvin temperatures. The results were compared to natural bulk Cu₂O as benchmark (crystal originates from a geological sample used in previous literature²³). Spectra normalized to the yellow 1s orthoexciton emission that were acquired at a laser power of 50 μ W (corresponding to a peak intensity of 3 kW/cm²) and an excitation wavelength of 532 nm are presented in Fig.2a, showing considerably reduced emission related to oxygen vacancies for the case of Cu₂O microcrystals. An emission feature around 1.95 eV was observed for both Cu₂O microcrystals and the natural bulk sample, which has been reported repeatedly in literature. It was attributed to phonon-assisted transitions and defect emission in close spectral proximity^{12,24,25} with the latter potentially being correlated with local strain in the sample²⁶. Additional data for different samples and natural bulk crystal positions can be found in Supplementary Fig.S4. Low point defect densities are highly important for efficient cooling of the exciton gas in Cu₂O as trapping at defects is a limiting factor for exciton lifetimes. The latter were found to be significantly shortened for increasing oxygen vacancy concentrations²⁷. Furthermore, it has been suggested that relaxation processes involving vacancies can lead to heating due to phonon emission²⁴, which is detrimental for achieving cold exciton gas temperatures. In addition to intrinsic point defects, excitons and their luminescence properties may be influenced by the presence of extrinsic impurities. The latter can lead to the formation of bound excitons, which show multiple emission lines in the energy range around \sim 2.00 eV, below the phonon-assisted orthoexciton transition²⁸. In Fig.2b we directly compare photoluminescence spectra obtained from synthetic Cu₂O microcrystals and from the natural bulk crystal under identical experimental conditions (excitation power 50 nW). It is evident that all peak-like features related to excitons bound to extrinsic impurities are absent in Cu₂O microcrystals, once more validating the excellent purity and material quality of our samples. Moreover, we assess the energy level structure of yellow 1s excitons in Cu₂O microcrystals by monitoring luminescence from different phonon-assisted transitions (Fig.2c). The emission features were assigned according to previous literature²⁹ and the energy splitting of 1s excitons into orthoexcitons and paraexcitons separated by 12 meV in unstrained Cu₂O was validated. The influence of strain on the luminescence spectra of Cu₂O microcrystals is discussed in Supplementary Fig.S5. Exciton relaxation was further studied by assessing its excitation power dependence. For this purpose, the incident laser power was varied and the luminescence spectra were integrated in an energy range covering bound excitons, phonon-assisted transitions and the direct quadrupole line (Fig.2d). The integrated intensity of the Cu₂O microcrystal is in excellent agreement with a linear relationship (slope 0.995 ± 0.008) for excitation powers spanning over more than two orders of magnitude, showing slight sub-linear behaviour at elevated excitation levels. On the other hand, deviations from a linear power dependence were significantly more pronounced for the natural bulk crystal. Sub-linear power dependence of excitonic emissions in Cu₂O has been previously observed in experiments using natural bulk samples^{28,30–32} and synthetic crystals grown by the floating zone method³³ using various types of laser excitation. It has been attributed to an efficient non-radiative two-body recombination process, which can be explained by Auger decay³⁴, by the formation of short-lived biexcitons³⁵ or by exciton interconversion via spin exchange³⁶. The estimated recombination rates reported in literature vary considerably as the process is expected to be sensitive to Cu₂O crystal symmetry and the resulting band structure; hence it has been anticipated that Auger recombination is associated with broken band symmetries in the vicinity of impurities⁶, which would explain the less pronounced two-body decay in low-defect-density Cu₂O microcrystals. Hence, we consider the latter an ideal platform for studying high-density exciton gases and their quantum statistics, which will be detailed in the next section.

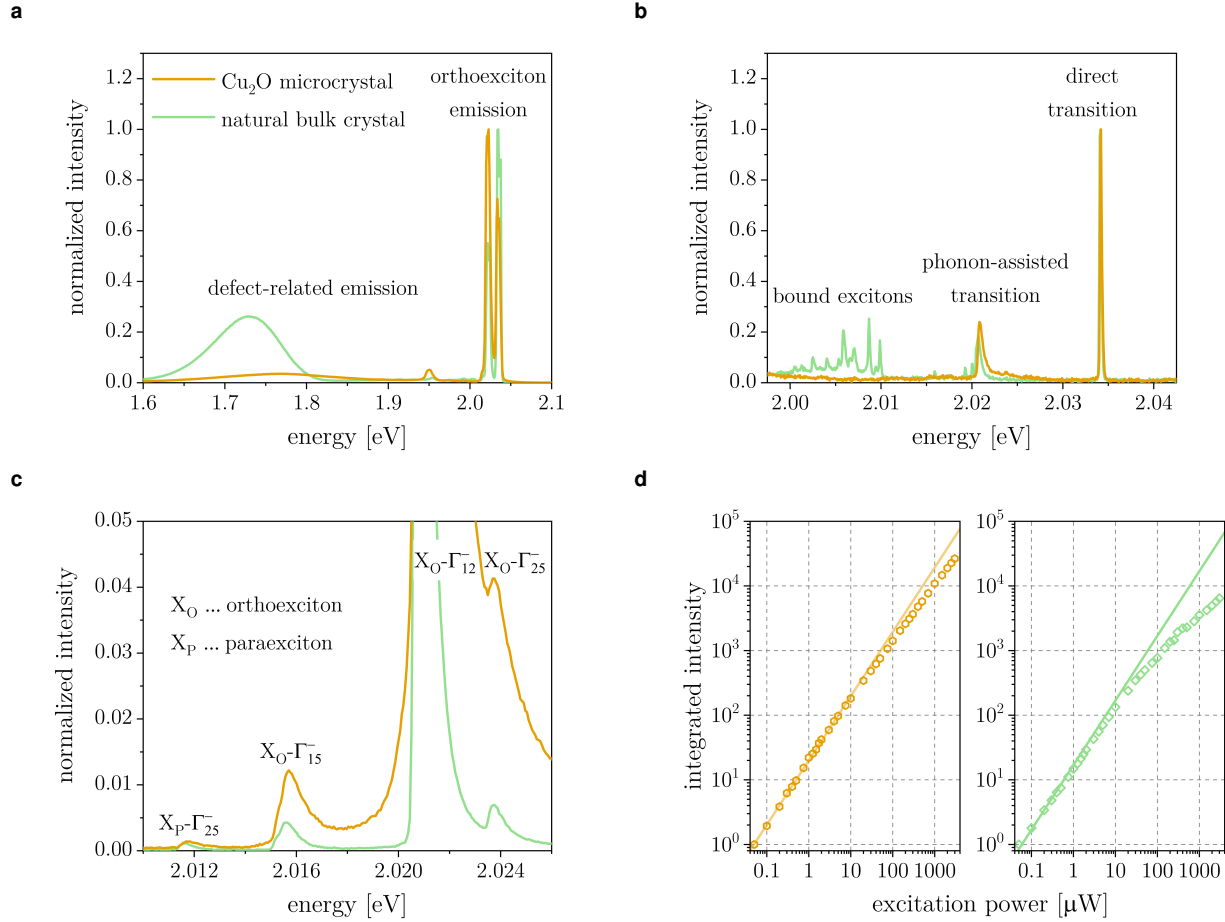


Fig.2 | Photoluminescence spectroscopy of Cu₂O microcrystals at milli-Kelvin temperatures benchmarked to measurements on a natural bulk crystal. **a**, Normalized photoluminescence of excitons and point defects (excitation power 50 μW). **b**, Emission from different excitonic transitions and bound excitons at low excitation power of 50 nW (spectra normalized to direct transition). **c**, Phonon-assisted transitions of ortho- and paraexcitons (spectra normalized to direct transition; excitation power 50 μW). **d**, Excitation power dependence of integrated emission in an energy range covering bound excitons, phonon-assisted transitions and the direct quadrupole line. Solid lines are a linear fit (Cu₂O microcrystal, left) and a linear curve as guide to the eye (natural bulk crystal, right), respectively.

Quantum-degeneracy of 1s ortho- and paraexcitons

Cu₂O has been considered the prime candidate for excitonic Bose-Einstein condensation in three-dimensional semiconductors due to several favourable properties, including large exciton binding energies of 150 meV, small Bohr radii around 0.7 nm leading to high Mott transition densities, as well as the same positive parity of the highest valence band and the lowest conduction band decoupling the exciton ground state (paraexciton) from photon interactions. Paraexcitons are thus particularly relevant for experiments related to Bose-Einstein condensation and have been predominantly studied using strain-induced confining potentials realized by the Hertzian stress technique of pressing a spherical object against a flat Cu₂O crystal surface^{31,37–39}. Decades of research on natural bulk samples have resulted in several reports of quantum degeneracy and Bose-Einstein condensation, which have been questioned by competing models assuming efficient two-body Auger recombination, inhomogeneous exciton distributions and exciton diffusion effects in macroscopic crystals⁶. We address this controversy by studying the exciton gas properties in Cu₂O microcrystals as a new experimental configuration providing confined geometries.

Photoluminescence spectroscopy was performed on single Cu₂O microcrystals in a dilution refrigerator using continuous-wave green laser excitation (532 nm), in particular analyzing the lineshape of the X_O – Γ₁₂ phonon-assisted orthoexciton transition. Three spectra acquired at laser input powers of 50 nW, 5 μW and 500 μW are presented in Fig.3a together with fits using a Bose-Einstein distribution function in excellent agreement with the experimental lineshape. Extracted fit parameters for the chemical potential μ and the exciton gas temperature T are shown in Fig.3b for excitation powers covering four orders of magnitude. Up to laser input powers of 10 μW, the chemical potential was very close to zero ($\mu=0$ corresponds to the phase transition to a Bose-Einstein condensate), while the exciton gas temperature remained almost constant with values around 9 K. The orthoexciton gas was gradually leaving the quantum-degenerate regime above excitation levels of 10 μW, which coincides

with deviations from the linear power dependence of orthoexciton luminescence (cf. Fig. 2d). Additional data obtained from a different Cu₂O microcrystal with consistent orthoexciton gas characteristics is presented in Supplementary Fig. S6. Most interestingly, the extracted fit parameters suggest a different exciton gas behaviour compared to previous literature, where a quantum saturation effect was repeatedly observed with the exciton gas moving along adiabats parallel to the phase boundary of Bose-Einstein condensation^{1,1,41}. It was argued that the continuous temperature increase with increasing exciton density is associated with heating via two-body Auger decay. Here, the extracted fit parameters suggest increasing levels of quantum degeneracy and hence higher exciton densities for decreasing laser excitation at almost constant exciton gas temperatures. For natural bulk crystals, lineshapes suggesting quantum-degenerate statistics were attributed to a superposition of classical Maxwell-Boltzmann distributions as a result of exciton diffusion over several tens of micrometers⁴². In our case, we can exclude this potential explanation due to the small sizes of the Cu₂O microcrystals. Further experimental and theoretical work will be required to assess if the presented orthoexciton gas characteristics are linked with Bose-Einstein condensation and to exclude possible alternative explanations, such as density-dependent recombination mechanisms or deviations from the ideal Bose gas theory. Our surprising results provide important new insights stimulating the use of Cu₂O microcrystals as experimental platform in future studies, which will be required to unambiguously solve the enigma of quantum-degenerate statistics and Bose-Einstein condensation of orthoexcitons in Cu₂O.

Furthermore, we demonstrate that paraexcitons are also in the quantum-degenerate regime by analyzing the lineshape of the phonon-assisted $X_P - \Gamma_{25}^-$ transition. Three spectra acquired under laser input powers of 10 μ W, 20 μ W and 40 μ W and the corresponding Bose-Einstein fits are shown in Fig. 3c. We obtained high degrees of quantum degeneracy with fit values of the chemical potential μ around $-0.1 kT$ and the temperature T around 5 K (10 μ W excitation). For increasing laser input powers, μ gradually decreased whereas T increased. Note that deviations from the fit can be attributed to a phonon-assisted orthoexciton transition at higher energies (see also Fig. 2c). Considering our results on orthoexcitons described above, Cu₂O microcrystals are capable of hosting quantum gas mixtures with intricate coupling between their components (spin-flip and spin-exchange processes^{36,43} of ortho- and paraexcitons) in confined geometries, providing new directions for future theoretical and experimental work. Moreover, the demonstration of quantum-degenerate paraexcitons in Cu₂O microcrystals render the latter a promising platform for exploring excitonic Bose-Einstein condensation in unprecedented device architectures, e.g. employing configurations for dynamic strain tuning by means of piezoelectric substrates⁴⁴.

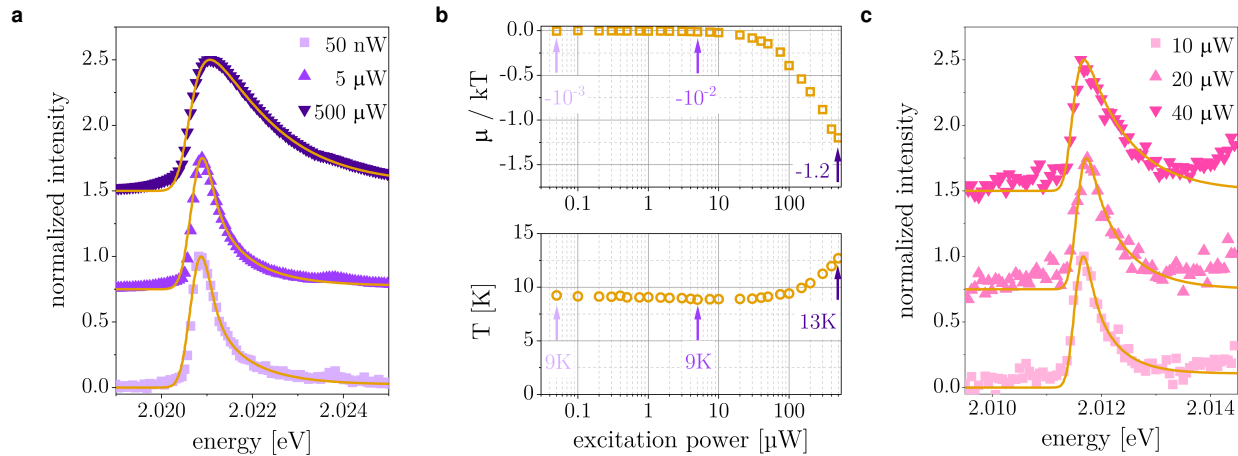


Fig.3 | Quantum-degenerate exciton gas in Cu₂O microcrystals. **a**, Photoluminescence spectra of phonon-assisted $X_O - \Gamma_{12}^-$ orthoexciton emission for three different excitation powers. The solid lines correspond to fits using a Bose-Einstein distribution function (spectra were offset vertically for clarity). **b**, Extracted fit parameters for the chemical potential μ and the temperature T of the orthoexciton gas for excitation powers covering four orders of magnitude. The parameters for the spectra shown in **a**, are annotated in the graph. **c**, Phonon-assisted $X_P - \Gamma_{25}^-$ paraexciton transition for three different excitation powers with fits using a Bose-Einstein distribution function (spectra were offset vertically for clarity). Details on the obtained fit parameters are described in the text.

Rydberg excitons - the yellow np series

After initial experiments in the middle of the last century, Rydberg excitons in Cu₂O have recently attracted considerable attention due to the experimental demonstration of principal quantum numbers up to $n=25$ in absorption measurements using natural bulk crystals³. The question arises if Rydberg states can also be observed in the Cu₂O microcrystals presented here, which was assessed by means of photoluminescence experiments. Results obtained for varying incident laser powers are presented in Fig. 4a (spectra normalized to their respective maxima). Emission peaks corresponding to Rydberg excitons up to $n=6$ were identified at low and intermediate excitation, which can also be seen in the exemplary spectrum shown in Fig. 4b. The high energy tail approaching the band gap could indicate the presence of higher-lying Rydberg excitons, which exhibit

considerable spectral overlap due to their broadened luminescence linewidth. The $2p$ peak showed a markedly asymmetric lineshape consistent with previous literature on bulk Cu_2O crystals^{25,45,46}, whereas the relative emission intensities from np states differed in our case. The minor peak between the $2p$ and $3p$ energy level is attributed to s -type excitons²⁵. Rydberg exciton emission showed broadening for increasing excitation power, which can be explained by a combination of phonon scattering and density-dependent effects⁴⁵; the red shift indicates a bandgap decrease due to laser-induced sample heating. Most importantly, the power-dependent measurements verify the robustness of Rydberg excitons in Cu_2O microcrystals as their emission was detected in a wide range of excitation conditions. Additional photoluminescence spectroscopy data is shown in Supplementary Fig.S7, validating that Rydberg excitons could be consistently observed in Cu_2O microcrystal samples.

Furthermore, site-controlled Cu_2O microstructures (Fig.4c) were achieved by lithographic patterning of the copper film before oxidation. We demonstrate luminescence from excited Rydberg states in a circular Cu_2O microstructure with $5\mu\text{m}$ diameter (Fig.4d). The intensity ratio of np states was different compared to Cu_2O microcrystals, which could be explained by variations in microscopic strain⁴⁶. The Rydberg exciton energies were evaluated as a function of n^{-2} for results obtained from site-controlled microstructures, from not site-controlled microcrystals and from a natural bulk crystal (Fig.4e). Excellent agreement with a linear relation was found and exciton binding energies of 98 meV and 97 meV were deduced for the synthetic samples and the natural bulk crystal, respectively. The extracted exciton binding energies concur with previous findings using bulk crystals, obtained from both photoluminescence (97 meV⁴⁵; 98.5 meV⁴⁶) and absorption measurements (98 meV⁴⁷). Hence our results demonstrate the realization of site-controlled, micrometer-sized Cu_2O structures as host platform for Rydberg excitons on silicon, opening up opportunities for unprecedented photonic device architectures. For instance, our technology will enable applications in nonlinear quantum optics relying on interactions between Rydberg states⁴⁸, as clear signatures of the Rydberg blockade effect have been recently reported for principal quantum numbers around $n=6$ ¹⁸. We expect that in the presented synthetic Cu_2O samples the observation of Rydberg states with higher principal quantum number n is not limited by material quality but is hampered by luminescence broadening, similar to previous reports on natural crystals⁴⁵, suggesting future experiments in an absorption geometry.

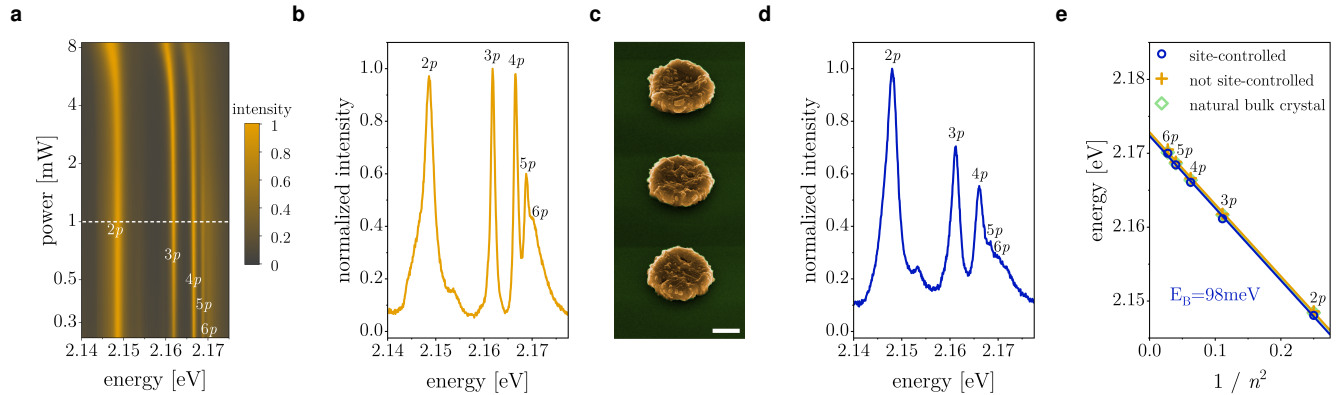


Fig.4 | Rydberg excitons in Cu_2O microcrystals and site-controlled structures. **a**, Normalized photoluminescence of np Rydberg exciton emission from Cu_2O microcrystal for varying excitation powers. The white dashed line indicates the spectrum presented in **b**, which was acquired at an excitation power of 1 mW and a cryostat stage temperature around 1.8 K. **c**, Scanning electron micrograph of site-controlled circular Cu_2O microstructures with $5\mu\text{m}$ diameter (scale bar $2\mu\text{m}$; sample tilt 45°). **d** Photoluminescence spectrum of site-controlled Cu_2O microstructure that was acquired under identical experimental conditions as in **b**. **e**, Rydberg exciton energies as a function of n^{-2} and the corresponding linear fits to extract the exciton binding energy E_B .

Conclusion

We have presented the growth of Cu_2O microcrystals on silicon substrates, showing excellent optical material quality with exceedingly low point defect and impurity levels. The fabrication method for obtaining high-quality Cu_2O films via a scalable thermal oxidation process has guiding significance for diverse areas where this low-cost, non-toxic material is employed, such as photovoltaics and photocatalysis. Cu_2O microcrystals were identified as ideal host material for dense exciton gases at milli-Kelvin temperatures, in particular $1s$ ortho- and paraexcitons exhibiting kinetic energy distributions obeying Bose-Einstein statistics. Excitons in the quantum-degenerate regime were obtained through continuous-wave laser excitation of confined micrometer-sized geometries, which constitutes an entirely new approach for assessing the feasibility of excitonic Bose-Einstein condensation in this material. Furthermore, the demonstration of Rydberg excitons in Cu_2O microcrystals and their integration on silicon have far-reaching implications for future applications in photonic quantum information processing. For instance, Rydberg states in Cu_2O have been proposed for the realization of novel solid-state single-photon sources⁴⁹ and giant optical nonlinearities⁵⁰. Hence our work lays the foundation for a platform technology enabling solid-state Rydberg excitations on-chip, which is envisioned to result in integrated devices capable of generating and manipulating light at the single photon level.

Methods

Growth of Cu₂O microcrystals on silicon substrates

The deposition of copper films (thickness ~700 nm) was performed by electron beam evaporation onto pieces of silicon wafers with 150 nm thermal SiO₂. A thin intermediate titanium layer (thickness ~5 nm) was employed to improve the film adhesion on the substrate surface. Samples with structured Cu₂O were realized by patterning the copper film using an electron beam lithography lift-off process. Thermal oxidation was carried out in a tube furnace connected to a vacuum pump. Before growth experiments the system was evacuated and purged multiple times using high-purity synthetic air (Air Liquide Alphagaz 2). Cu₂O samples were grown by thermal oxidation at a pressure around 1 mbar and setpoint temperatures of 800°C or 850°C. The temperature was kept constant for 1 h or 5 h after reaching the setpoint value, followed by natural sample cool-down.

Sample characterization

The morphologies of Cu₂O films and microstructures were characterized by scanning electron microscopy imaging of the sample surfaces and of cross-sections obtained by mechanical cleaving. X-ray diffraction measurements were performed by specular scans using a PANalytical Empyrean system. Radiation from a sealed copper tube was used in combination with a secondary graphite monochromator in Bragg–Brentano geometry. Phase analysis was carried out relying on powder patterns from the database PDF2, International Center for Diffraction Data, using 004-0836 for Cu and 005-0667 for Cu₂O.

Photoluminescence spectroscopy and data evaluation

All photoluminescence spectroscopy experiments were performed using a Horiba iHR550 spectrometer and a continuous-wave, diode-pumped solid-state laser emitting at 532 nm. Room-temperature spectra were acquired using an objective (NA=0.82) for excitation and collection. Spectroscopy at milli-Kelvin temperatures was performed relying on a cryogen-free dilution refrigerator (Bluefors) with a base temperature around 10 mK. Optical side-access windows with anti-reflective coatings were used for laser excitation of the samples mounted on a dedicated stage controlled by piezoelectric actuators, which had a base temperature around 40 mK. The laser was focused by a lens (NA=0.50) inside the cryostat to a spot diameter around 1.2 μm (full width at half maximum); the power was measured at the outermost cryostat window. Spectroscopy results on phonon-assisted ortho- and paraexciton emission at milli-Kelvin temperatures were fitted using a Bose-Einstein distribution function. Convolution with a Gaussian function (orthoexcitons $\sigma=0.20$ meV; paraexcitons $\sigma=0.12$ meV) was considered to account for additional broadening by the linewidth of the direct orthoexciton transition and by the spectrometer resolution.

References

1. Snoke, D., Wolfe, J. P. & Mysyrowicz, A. Quantum saturation of a bose gas: Excitons in Cu₂O. *Phys. Rev. Lett.* **59**, 827–830 (1987). DOI 10.1103/PhysRevLett.59.827.
2. Snoke, D. W., Wolfe, J. P. & Mysyrowicz, A. Evidence for Bose-Einstein condensation of a two-component exciton gas. *Phys. Rev. Lett.* **64**, 2543–2546 (1990). DOI 10.1103/PhysRevLett.64.2543.
3. Kazimierczuk, T., Fröhlich, D., Scheel, S., Stolz, H. & Bayer, M. Giant Rydberg excitons in the copper oxide Cu₂O. *Nature* **514**, 343–347 (2014). DOI 10.1038/nature13832.
4. Grünwald, P. *et al.* Signatures of quantum coherences in Rydberg excitons. *Phys. Rev. Lett.* **117**, 133003 (2016). DOI 10.1103/PhysRevLett.117.133003.
5. Aßmann, M., Thewes, J., Fröhlich, D. & Bayer, M. Quantum chaos and breaking of all anti-unitary symmetries in Rydberg excitons. *Nat. Mater.* **15**, 741–745 (2016). DOI 10.1038/NMAT4622.
6. Snoke, D. & Kavoulakis, G. M. Bose–Einstein condensation of excitons in Cu₂O: progress over 30 years. *Rep. Prog. Phys.* **77**, 116501 (2014). DOI 10.1088/0034-4885/77/11/116501.
7. Wu, S.-C., Tan, C.-S. & Huang, M. H. Strong facet effects on interfacial charge transfer revealed through the examination of photocatalytic activities of various Cu₂O–ZnO heterostructures. *Adv. Funct. Mater.* **27**, 1604635 (2017). DOI 10.1002/adfm.201604635.
8. Pan, L. *et al.* Boosting the performance of Cu₂O photocathodes for unassisted solar water splitting devices. *Nat. Catal.* **1**, 412–420 (2018). DOI 10.1038/s41929-018-0077-6.
9. Minami, T., Nishi, Y. & Miyata, T. Efficiency enhancement using a Zn_{1-x}Ge_x-O thin film as an n-type window layer in Cu₂O-based heterojunction solar cells. *Appl. Phys. Express* **9**, 052301 (2016). DOI 10.7567/APEX.9.052301.
10. Meyer, B. K. *et al.* Binary copper oxide semiconductors: From materials towards devices. *physica status solidi (b)* **249**, 1487–1509 (2012). DOI 10.1002/pspb.201248128.
11. Li, J. *et al.* Engineering of optically defect free Cu₂O enabling exciton luminescence at room temperature. *Opt. Mater. Express* **3**, 2072–2077 (2013). DOI 10.1364/OME.3.002072.
12. Kracht, M., Schörmann, J. & Eickhoff, M. Plasma assisted molecular beam epitaxy of Cu₂O on MgO(001): Influence of copper flux on epitaxial orientation. *J. Cryst. Growth* **436**, 87–91 (2016). DOI 10.1016/j.jcrysgro.2015.11.041.
13. Brittman, S. *et al.* Epitaxially aligned cuprous oxide nanowires for all-oxide, single-wire solar cells. *Nano Lett.* **14**, 4665–4670 (2014). DOI 10.1021/nl501750h.

14. Yin, Z. G. *et al.* Two-dimensional growth of continuous Cu₂O thin films by magnetron sputtering. *Appl. Phys. Lett.* **86**, 061901 (2005). DOI 10.1063/1.1861117.
15. Bergum, K. *et al.* Improving carrier transport in Cu₂O thin films by rapid thermal annealing. *J. Physics: Condens. Matter* **30**, 075702 (2018). DOI 10.1088/1361-648X/aaa5f4.
16. Mani, S., Jang, J., Ketterson, J. & Park, H. High-quality Cu₂O crystals with various morphologies grown by thermal oxidation. *J. Cryst. Growth* **311**, 3549–3552 (2009). DOI 10.1016/j.jcrysgro.2009.05.006.
17. Chang, K. B., Frazer, L., Schwartz, J. J., Ketterson, J. B. & Poeppelmeier, K. R. Removal of copper vacancies in cuprous oxide single crystals grown by the floating zone method. *Cryst. Growth & Des.* **13**, 4914–4922 (2013). DOI 10.1021/cg401081m.
18. Heckötter, J. *et al.* Rydberg excitons in the presence of an ultralow-density electron-hole plasma. *Phys. Rev. Lett.* **121**, 097401 (2018). DOI 10.1103/PhysRevLett.121.097401.
19. Zhou, G. *et al.* In situ atomic-scale visualization of oxide islanding during oxidation of Cu surfaces. *Chem. Commun.* **49**, 10862–10864 (2013). DOI 10.1039/C3CC46684A.
20. Luo, L., Kang, Y., Yang, J. C. & Zhou, G. Effect of oxygen gas pressure on orientations of Cu₂O nuclei during the initial oxidation of Cu(100), (110) and (111). *Surf. Sci.* **606**, 1790–1797 (2012). DOI 10.1016/j.susc.2012.07.042.
21. Gattinoni, C. & Michaelides, A. Atomistic details of oxide surfaces and surface oxidation: the example of copper and its oxides. *Surf. Sci. Reports* **70**, 424–447 (2015). DOI 10.1016/j.surfrep.2015.07.001.
22. LaGrow, A. P., Ward, M. R., Lloyd, D. C., Gai, P. L. & Boyes, E. D. Visualizing the Cu/Cu₂O interface transition in nanoparticles with environmental scanning transmission electron microscopy. *J. Am. Chem. Soc.* **139**, 179–185 (2017). DOI 10.1021/jacs.6b08842.
23. Mysyrowicz, A., Hulin, D. & Antonetti, A. Long exciton lifetime in Cu₂O. *Phys. Rev. Lett.* **43**, 1123–1126 (1979). DOI 10.1103/PhysRevLett.43.1123.
24. Frazer, L., Chang, K. B., Schaller, R. D., Poeppelmeier, K. R. & Ketterson, J. B. Vacancy relaxation in cuprous oxide (Cu_{2-x}O_{1-y}). *J. Lumin.* **183**, 281–290 (2017). DOI 10.1016/j.jlumin.2016.11.011.
25. Takahata, M. & Naka, N. Photoluminescence properties of the entire excitonic series in Cu₂O. *Phys. Rev. B* **98**, 195205 (2018). DOI 10.1103/PhysRevB.98.195205.
26. Frazer, L. *et al.* Evaluation of defects in cuprous oxide through exciton luminescence imaging. *J. Lumin.* **159**, 294–302 (2015). DOI 10.1016/j.jlumin.2014.11.035.
27. Koirala, S., Naka, N. & Tanaka, K. Correlated lifetimes of free paraexcitons and excitons trapped at oxygen vacancies in cuprous oxide. *J. Lumin.* **134**, 524–527 (2013). DOI 10.1016/j.jlumin.2012.07.035.
28. Jang, J. I., Sun, Y., Watkins, B. & Ketterson, J. B. Bound excitons in Cu₂O: Efficient internal free exciton detector. *Phys. Rev. B* **74**, 235204 (2006). DOI 10.1103/PhysRevB.74.235204.
29. Mysyrowicz, A., Trauernicht, D. P., Wolfe, J. P. & Trebin, H. R. Stress dependence of the paraexciton in Cu₂O. *Phys. Rev. B* **27**, 2562–2564 (1983). DOI 10.1103/PhysRevB.27.2562.
30. O'Hara, K. E., Gullingsrud, J. R. & Wolfe, J. P. Auger decay of excitons in Cu₂O. *Phys. Rev. B* **60**, 10872–10885 (1999). DOI 10.1103/PhysRevB.60.10872.
31. Trauernicht, D. P., Wolfe, J. P. & Mysyrowicz, A. Thermodynamics of strain-confined paraexcitons in Cu₂O. *Phys. Rev. B* **34**, 2561–2575 (1986). DOI 10.1103/PhysRevB.34.2561.
32. Stolz, H. *et al.* Condensation of excitons in Cu₂O at ultracold temperatures: experiment and theory. *New J. Phys.* **14**, 105007 (2012). DOI 10.1088/1367-2630/14/10/105007.
33. Karpinska, K., Mostovoy, M., van der Vegte, M. A., Revcolevschi, A. & van Loosdrecht, P. H. M. Decay and coherence of two-photon excited yellow orthoexcitons in Cu₂O. *Phys. Rev. B* **72**, 155201 (2005). DOI 10.1103/PhysRevB.72.155201.
34. Wolfe, J. P. & Jang, J. I. The search for Bose–Einstein condensation of excitons in Cu₂O: exciton-Auger recombination versus biexciton formation. *New J. Phys.* **16**, 123048 (2014). DOI 10.1088/1367-2630/16/12/123048.
35. Jang, J. I. & Wolfe, J. P. Auger recombination and biexcitons in Cu₂O: A case for dark excitonic matter. *Phys. Rev. B* **74**, 045211 (2006). DOI 10.1103/PhysRevB.74.045211.
36. Kavoulakis, G. M. & Mysyrowicz, A. Auger decay, spin exchange, and their connection to Bose-Einstein condensation of excitons in Cu₂O. *Phys. Rev. B* **61**, 16619–16622 (2000). DOI 10.1103/PhysRevB.61.16619.
37. Yoshioka, K., Chae, E. & Kuwata-Gonokami, M. Transition to a Bose–Einstein condensate and relaxation explosion of excitons at sub-Kelvin temperatures. *Nat. Commun.* **2**, 328 (2011). DOI 10.1038/ncomms1335.
38. Schwartz, R., Naka, N., Kieseling, F. & Stolz, H. Dynamics of excitons in a potential trap at ultra-low temperatures: paraexcitons in Cu₂O. *New J. Phys.* **14**, 023054 (2012). DOI 10.1088/1367-2630/14/2/023054.
39. Fröhlich, D. & Bayer, M. Emission of Cu₂O paraexcitons confined by a strain trap: Hints of a Bose-Einstein condensate? *Phys. Solid State* **60**, 1600–1605 (2018). DOI 10.1134/S1063783418080061.

40. Lin, J. L. & Wolfe, J. P. Bose-Einstein condensation of paraexcitons in stressed Cu₂O. *Phys. Rev. Lett.* **71**, 1222–1225 (1993). DOI 10.1103/PhysRevLett.71.1222.
41. Snoke, D. W. & Wolfe, J. P. Picosecond dynamics of degenerate orthoexcitons in Cu₂O. *Phys. Rev. B* **42**, 7876–7884 (1990). DOI 10.1103/PhysRevB.42.7876.
42. O'Hara, K. E. & Wolfe, J. P. Relaxation kinetics of excitons in cuprous oxide. *Phys. Rev. B* **62**, 12909–12922 (2000). DOI 10.1103/PhysRevB.62.12909.
43. Jang, J. I., O'Hara, K. E. & Wolfe, J. P. Spin-exchange kinetics of excitons in Cu₂O: Transverse acoustic phonon mechanism. *Phys. Rev. B* **70**, 195205 (2004). DOI 10.1103/PhysRevB.70.195205.
44. Zeuner, K. D. *et al.* A stable wavelength-tunable triggered source of single photons and cascaded photon pairs at the telecom C-band. *Appl. Phys. Lett.* **112**, 173102 (2018). DOI 10.1063/1.5021483.
45. Kitamura, T., Takahata, M. & Naka, N. Quantum number dependence of the photoluminescence broadening of excitonic Rydberg states in cuprous oxide. *J. Lumin.* **192**, 808–813 (2017). DOI 10.1016/j.jlumin.2017.07.060.
46. Reimann, K. & Syassen, K. Raman scattering and photoluminescence in Cu₂O under hydrostatic pressure. *Phys. Rev. B* **39**, 11113–11119 (1989). DOI 10.1103/PhysRevB.39.11113.
47. Matsumoto, H., Saito, K., Hasuo, M., Kono, S. & Nagasawa, N. Revived interest on yellow-exciton series in Cu₂O: An experimental aspect. *Solid State Commun.* **97**, 125–129 (1996). DOI 10.1016/0038-1098(95)00601-X.
48. Firstenberg, O., Adams, C. S. & Hofferberth, S. Nonlinear quantum optics mediated by Rydberg interactions. *J. Phys. B: At. Mol. Opt. Phys.* **49**, 152003 (2016). DOI 10.1088/0953-4075/49/15/152003.
49. Khazali, M., Heshami, K. & Simon, C. Single-photon source based on Rydberg exciton blockade. *J. Phys. B: At. Mol. Opt. Phys.* **50**, 215301 (2017). DOI 10.1088/1361-6455/aa8d7c.
50. Walther, V., Johne, R. & Pohl, T. Giant optical nonlinearities from Rydberg excitons in semiconductor microcavities. *Nat. Commun.* **9**, 1309 (2018). DOI 10.1038/s41467-018-03742-7.

Acknowledgements

The authors thank Roland Resel for helpful discussions. The Quantum Nano Photonics Group at KTH acknowledges financial support from the Linnaeus Center in Advanced Optics and Photonics (ADOPT). M.A.M.V. acknowledges funding from the Swedish Research Council under grant agreement No. 2016-04527. V.Z. acknowledges funding by the European Research Council under grant agreement No. 307687 (NaQuOp) and the Swedish Research Council under grant agreement No. 638-2013-7152. The project was co-funded by Vinnova and FP7 (GROWTH 291795).

Author contributions statement

S.S., M.A.M.V. and V.Z. conceived the experiments, with input from A.M. M.A.M.V. designed and built the milli-Kelvin photoluminescence spectroscopy setup. S.S. performed material growth, SEM characterization and photoluminescence experiments. Data analysis and interpretation was performed by S.S. with support from M.A.M.V., A.M. and V.Z. XRD characterization and the corresponding analysis was performed by B.K. The project was supervised by M.A.M.V. and V.Z. The manuscript was written by S.S. with inputs from all authors.

Additional information

The authors declare no competing financial interests.

Supplementary Figures

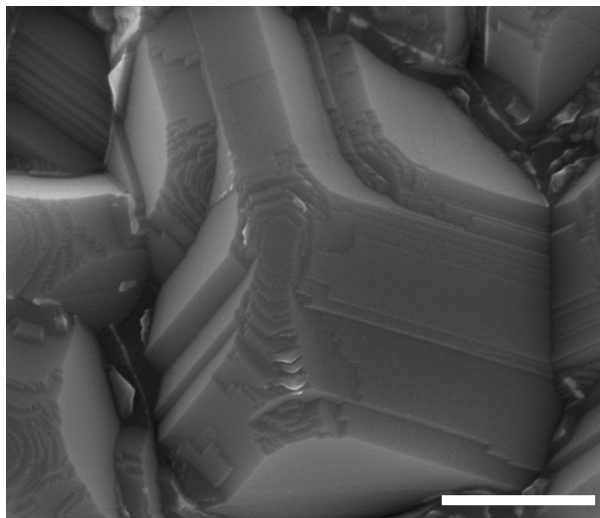


Fig.S1 | High-resolution scanning electron microscope image of Cu₂O microcrystal surface. Extended terrace-like structures suggest a two-dimensional growth mode for the individual microcrystals (scale bar 500 nm).

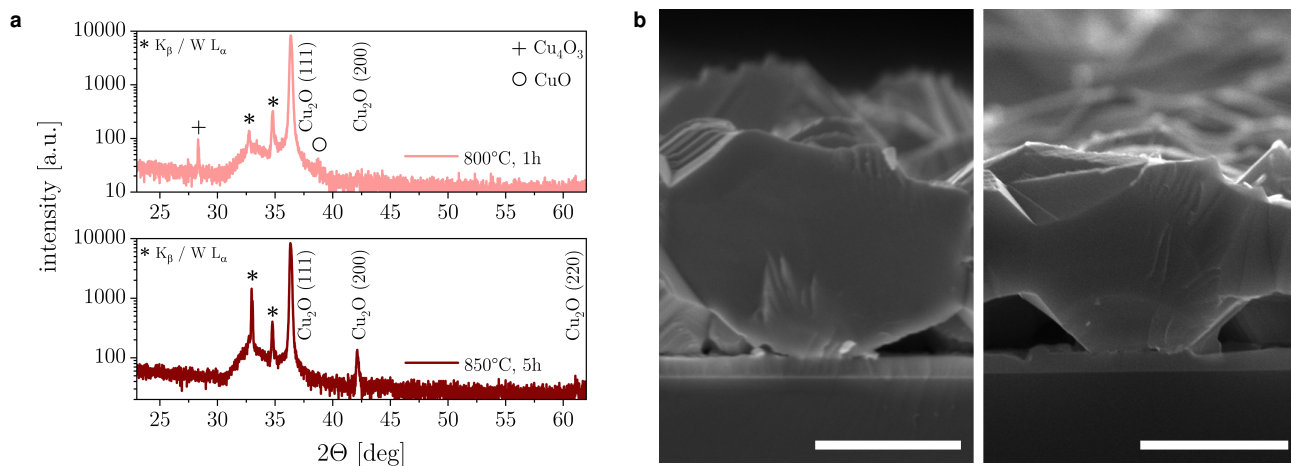


Fig.S2 | Characterization of Cu₂O microcrystal samples grown at different conditions. **a**, X-ray diffraction of films obtained through thermal oxidation at 800°C for 1 h and at 850°C for 5 h at pressures around 1 mbar of synthetic air. The former sample showed residual Cu₄O₃ and CuO phases, whereas in the latter sample phase-pure Cu₂O was found (database PDF2, International Center for Diffraction Data, using 005-0667 for Cu₂O, 049-1830 for Cu₄O₃ and 045-0937 for CuO). **b**, The corresponding cross-sectional scanning electron microscope images (left: 800°C / 1 h, right: 850°C / 5 h) show comparable Cu₂O microcrystal morphology (scale bars 1 μm). For the longer growth time a higher degree of intergrain connectivity was observed.

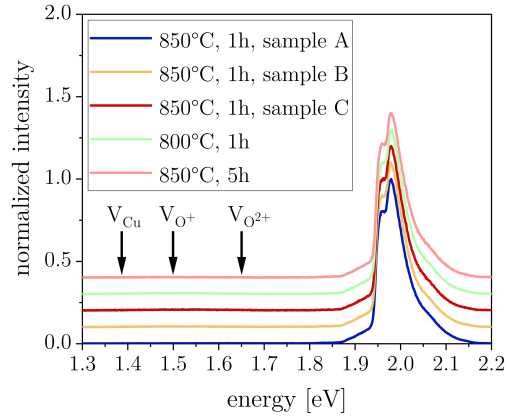


Fig.S3 | Room-temperature photoluminescence spectroscopy of excitons and point defects. The comparison of three samples obtained from different batches (850°C / 1 h) and two samples grown under different conditions (800°C / 1 h; 850°C / 5 h) show very similar excitonic emissions and no marked luminescence from point defects in all cases (spectra were offset vertically for clarity).

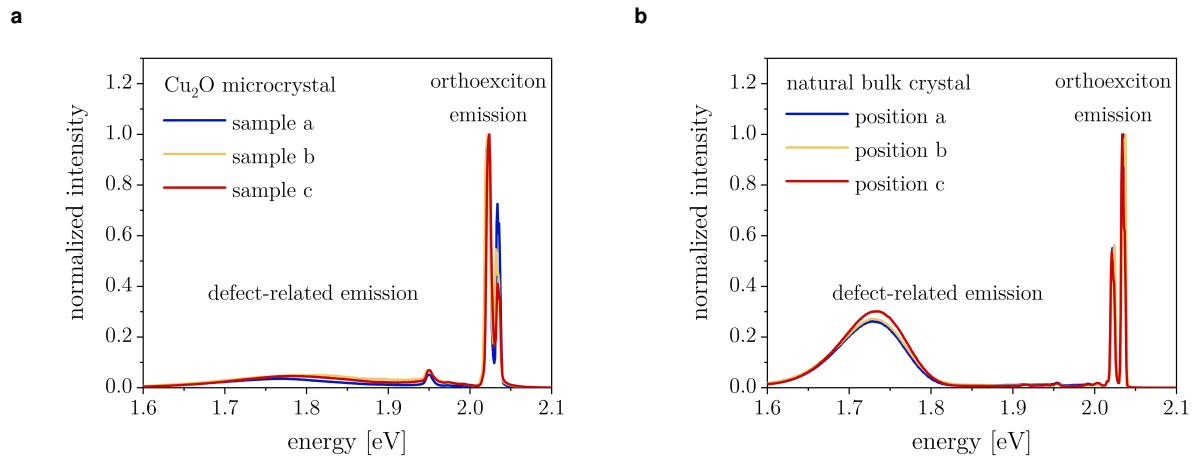


Fig.S4 | Photoluminescence spectroscopy of excitons and point defects at milli-Kelvin temperatures. **a.** Comparison of emission from Cu₂O microcrystals on three different samples (850°C / 1 h), which all show exceedingly low point defect levels. **b.** Comparison of three different sample positions on the natural bulk crystal, exhibiting comparable emission from oxygen vacancies. All measurements were performed at an excitation power of 50 μW.

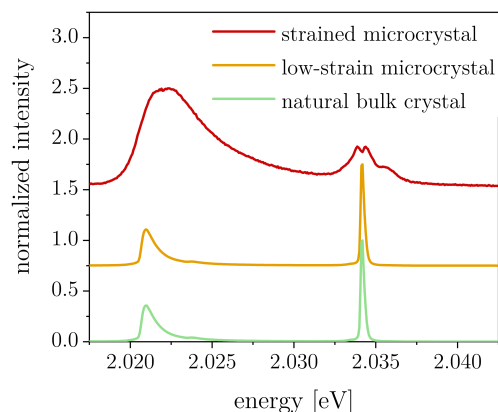


Fig.S5 |The influence of microscopic strain on excitons in Cu_2O microcrystals. Comparison of phonon-assisted and direct orthoexciton emission for strained Cu_2O microcrystal, low-strain Cu_2O microcrystal and the natural bulk crystal (excitation power $50 \mu\text{W}$; spectra vertically offset for clarity). Strained Cu_2O microcrystals exhibited a lifted energy degeneracy of the triplet orthoexciton state, similar to strained bulk crystals¹, with energy splittings around 1.5 meV, which is considerably smaller compared to previous reports on Cu_2O thin films epitaxially grown on MgO substrates^{2,3}. Stress values around 50 MPa were estimated from the experimental data assuming rhombohedral stress along the [110] direction⁴.

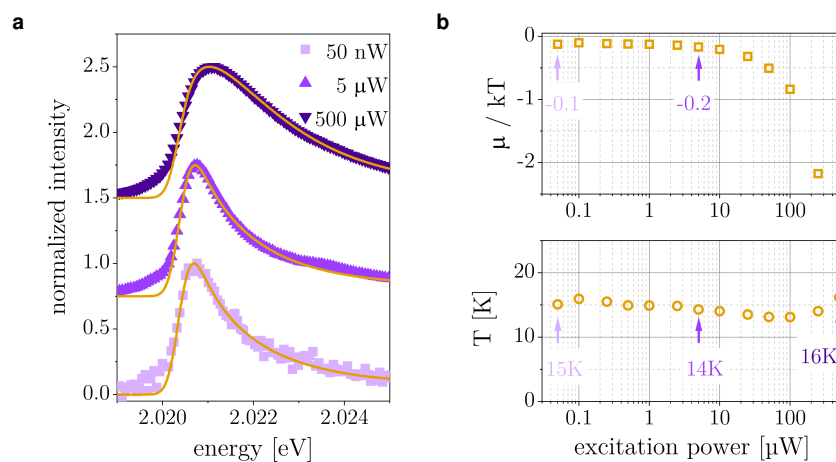


Fig.S6 |Quantum-degenerate orthoexciton gas in another Cu_2O microcrystal. Additional measurements were performed on a different sample grown under identical conditions. **a**, Photoluminescence spectra of phonon-assisted $X_O - \Gamma_{12}^-$ orthoexciton transition for three different excitation powers. The solid lines correspond to fits using a Bose-Einstein distribution function (spectra were offset vertically for clarity). **b**, Extracted fit parameters for the chemical potential μ and the temperature T of the orthoexciton gas for excitation powers covering four orders of magnitude. The parameters for the spectra shown in **a**, are annotated in the graph (The fit obtained for $500 \mu\text{W}$ excitation resulted in Maxwell-Boltzmann-like statistics and hence the value for the chemical potential is outside the plot range).

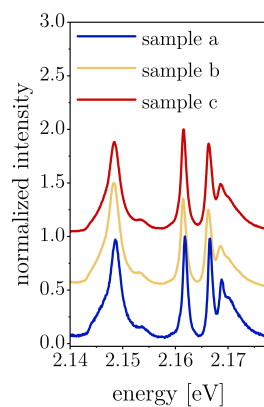


Fig.S7 | Luminescence from Rydberg excitons in Cu₂O microcrystals. Comparison of results obtained from three different samples (850°C / 1 h), exhibiting very similar characteristics (excitation power 1 mW; spectra vertically offset for clarity).

References

1. Lin, J. L. & Wolfe, J. P. Bose-Einstein condensation of paraexcitons in stressed Cu₂O. *Phys. Rev. Lett.* **71**, 1222–1225 (1993). DOI 10.1103/PhysRevLett.71.1222.
2. Sun, Y. *et al.* Strain splitting of 1s yellow orthoexciton of epitaxial orthorhombic Cu₂O films on MgO [110]. *Phys. Rev. B* **66**, 245315 (2002). DOI 10.1103/PhysRevB.66.245315.
3. Aihara, S. *et al.* Photoluminescence spectra and biaxial stress effects of yellow 1s excitons in Cu₂O thin films recrystallized epitaxially between paired MgO plates. *J. Lumin.* **167**, 211–215 (2015). DOI 10.1016/j.jlumin.2015.06.031.
4. Trebin, H. R., Cummins, H. Z. & Birman, J. L. Excitons in cuprous oxide under uniaxial stress. *Phys. Rev. B* **23**, 597–606 (1981). DOI 10.1103/PhysRevB.23.597.